



Toward a general tropical forest biomass prediction model from very high resolution optical satellite images



P. Ploton^{a,b,*}, N. Barbier^a, P. Couteron^a, C.M. Antin^a, N. Ayyappan^c, N. Balachandran^c, N. Barathan^c, J.-F. Bastin^d, G. Chuyong^e, G. Dauby^{f,g}, V. Droissart^{a,h}, J.-P. Gastellu-Etchegorryⁱ, N.G. Kamdem^j, D. Kenfack^k, M. Libalah^j, G. Mofack^l, S.T. Momo^{a,j}, S. Pargal^a, P. Petronelli^l, C. Proisy^{a,c}, M. Réjou-Méchain^{a,c}, B. Sonké^j, N. Texier^{a,j}, D. Thomas^m, P. Verley^a, D. Zebaze Dongmo^j, U. Bergerⁿ, R. Pélissier^{a,c}

^a AMAP Lab, IRD, CIRAD, CNRS, INRA, Montpellier University, Montpellier, France

^b Institut des sciences et industries du vivant et de l'environnement, Montpellier, France

^c French Institute of Pondicherry, Puducherry, India

^d Landscape Ecology and Plant Production Systems Unit, Université libre de Bruxelles, Brussels, Belgium

^e Department of Botany and Plant Physiology, University of Buea, Buea, Cameroon

^f Institut de Recherche pour le Développement, UMR-DIADE, Montpellier, France

^g Evolutionary Biology and Ecology, Faculté des Sciences, Université libre de Bruxelles, Brussels, Belgium

^h Herbarium et Bibliothèque de Botanique africaine, Université libre de Bruxelles, Brussels, Belgium

ⁱ Université Paul Sabatier, CESBIO, Toulouse, France

^j Laboratoire de Botanique systématique et d'Ecologie, Département des Sciences Biologiques, Ecole Normale Supérieure, Université de Yaoundé I, Yaoundé, Cameroon

^k Center for Tropical Forest Science — Forest Global Earth observatory, Smithsonian Tropical Research Institute, Washington, USA

^l Centre de coopération Internationale en Recherche Agronomique pour le Développement, UMR-ECOFOD, Kourou, France

^m Department of Biological Sciences, Washington State University, Vancouver, USA

ⁿ Technische Universität Dresden, Faculty of Environmental Sciences, Institute of Forest Growth and Forest Computer Sciences, Tharandt, Germany

ARTICLE INFO

Keywords:

Tropical forests
Canopy structure
Forest carbon
REDD
Passive optical imagery
Texture
Fourier transform
Lacunarity

ABSTRACT

Very high spatial resolution (VHSR) optical satellite imagery has shown good potential to provide non-saturating proxies of tropical forest aboveground biomass (AGB) from the analysis of canopy texture, for instance through the Fourier Transform Textural Ordination method. Empirical case studies however showed that the relationship between Fourier texture features and forest AGB varies across forest types and regions of the world, limiting model transferability. A better understanding of the biophysical mechanisms on which canopy texture – forest AGB relation relies is a prerequisite to move toward broad scale applications. Here we simulated VHSR optical canopy scenes in identical sun-sensor geometry for 279 1-ha tropical forest inventory plots distributed across the tropics. Our aim was to assess the respective merits and complementarity of two types of texture analysis techniques (i.e. Fourier and lacunarity) on a set of forests with contrasted structure and geographical origin, and develop a general texture-based approach for tropical forest AGB mapping. Across forests, Fourier texture captured a gradient of stands mean crown size reflecting well the progressive changes in stand structure throughout forest aggradation phase (e.g. Pearson's $r = -0.42$ with basal area) while lacunarity texture captured a gradient of canopy openness (i.e. Pearson's $r = -0.57$ with stand gap fraction). Both types of texture indices were highly complementary for predicting forest AGB at the global level (so-called FL-model). The residual error of the FL-model was structured across sites and could be partially captured with a bioclimatic proxy, further improving the performance of the global model (so-called FLE-model) and reducing site-level biases. The FLE model was tested on a set of real Pleiades images covering a mosaic of high-biomass forests in the Congo basin (mean AGB over 49 field plots: $359 \pm 98 \text{ Mg ha}^{-1}$), leading to a significant relationship ($R^2 = 0.47$ on validation data) with reasonable error levels ($< 25\%$ rRMSE). The increasing availability of VHSR optical sensors (such as from constellations of small satellite platforms) raises the possibility of routine repeated imaging

* Corresponding author at: IRD — UMR AMAP, Botany and Modeling of Architecture of Plants and Vegetations, Bd de la Lironde, TA A51/PS2, 34398 Montpellier Cedex 5, France.
E-mail address: p.ploton@gmail.com (P. Ploton).

of the world's tropical forests and suggests that texture-based analyses could become an essential tool in international efforts to monitor carbon emissions from deforestation and forest degradations (REDD +).

1. Introduction

Concerns about the effects of increasing atmospheric carbon dioxide on climate have led to an international initiative aiming at reducing forest-related emissions (Reducing Emissions from Deforestation and forest Degradation, REDD +), notably in the tropics where the bulk of global deforestation occurs (Pan et al., 2011). REDD + implementation fundamentally relies on our capacity to monitor forest carbon stock and dynamics at multiple spatial scales, from entire countries down to scales at which deforestation and degradation processes occur. In this context, remote sensing naturally becomes an essential tool (Baccini et al., 2012; DeFries et al., 2007; Saatchi et al., 2011). However, remote sensing of forest carbon stocks (often through forest aboveground biomass, hereafter denoted AGB) is challenging in the tropics because most satellite sensors are not sensitive to AGB variation above c. 150 Mg ha^{-1} , while AGB often exceeds 400 Mg ha^{-1} in tropical forests (Slik et al., 2013). This saturation is well documented for passive optical sensors of coarse

to intermediate spatial resolution such as the Moderate Resolution Imaging Spectroradiometer (MODIS) or Landsat Thematic Mapper (e.g. Lu, 2006; Lu et al., 2012; Zhao et al., 2016) but also for radar signals (notably L-band SAR, Mermoz et al., 2015), and thus constitutes a strong limit for those data types. In the past years, aircraft-based light detection and ranging systems have become popular for tropical forest AGB mapping, as their data appear to be free of saturation. Small-footprint airborne LiDAR data provide a detailed description of forest three-dimensional (3D) structure from which forest AGB can be estimated with good confidence (e.g. 14% relative error on 1-ha plots in Réjou-Méchain et al., 2015). Unfortunately this information comes at a cost rendering the wall-to-wall and regular coverage of large territories uneconomical (Erdody and Moskal, 2010; Messinger et al., 2016) or is even impossible to collect in some countries because of flight restrictions. An interesting alternative to airborne LiDAR may be found in very high spatial resolution (VHSR) optical images, as they are routinely captured by a variety of satellite platforms and therefore represent

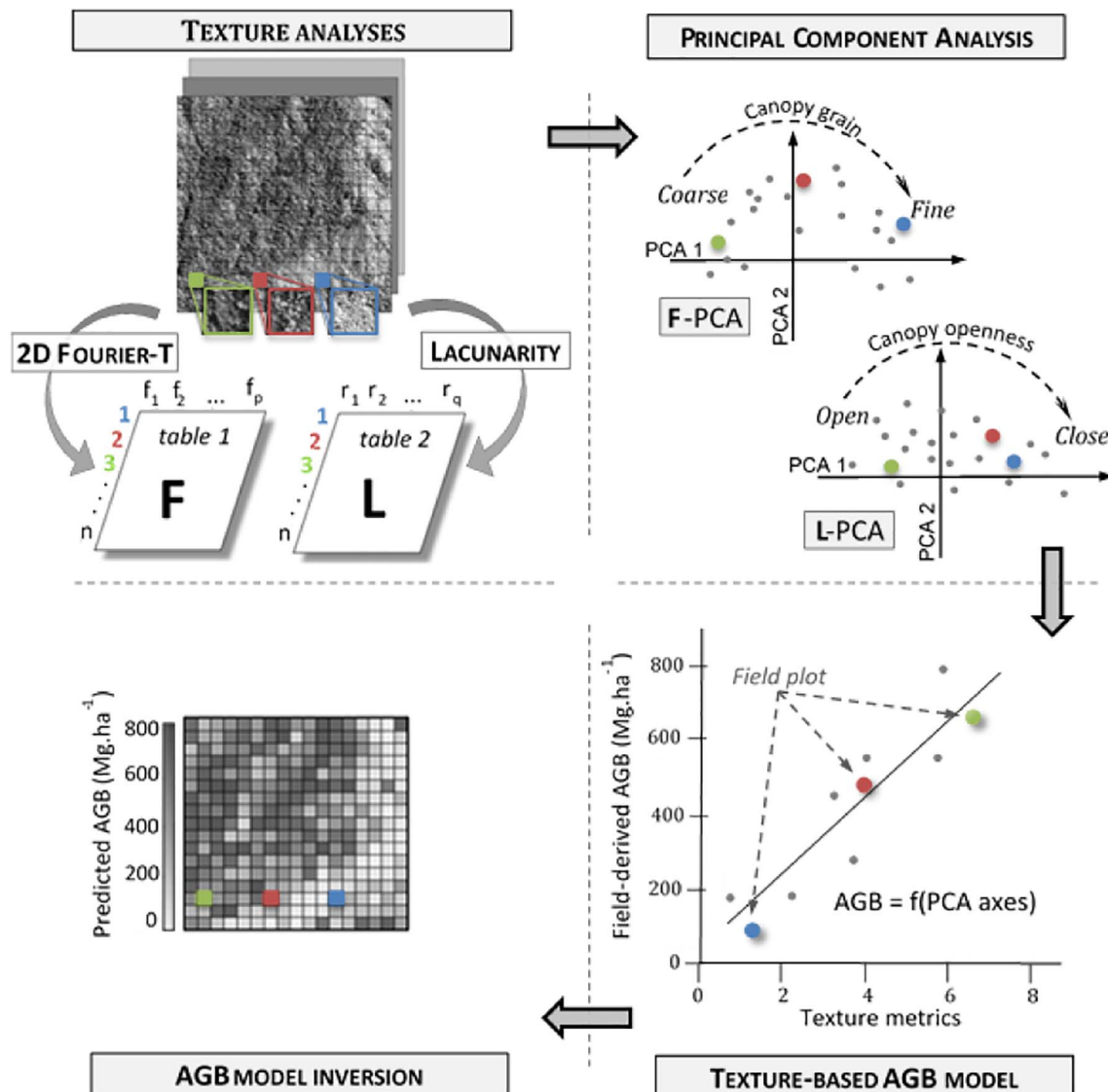


Fig. 1. Typical workflow of texture-based AGB mapping method.

an independent, affordable source of data for large-scale monitoring of tropical forests. The improvement brought by the increased spatial resolution over coarser, widely-used optical data (e.g. Landsat), lies on a fundamental change in the analysis: at metric to sub-metric resolutions, individual trees are now discernable in the image, allowing one to exploit the geometric properties of tree crowns (i.e. crown delineation algorithms, e.g. Broadbent et al., 2008; Zhou et al., 2013) or of forest canopies (i.e. texture analysis, e.g. Couteron et al., 2005) that conceptually more directly relate to stand biomass than spectral greenness indices.

Texture analysis of panchromatic VHSR canopy images either captured by optical satellite sensors (e.g. Couteron, 2002; Couteron et al., 2005) or derived from LiDAR canopy height models (e.g. Frazer et al., 2005; Véga et al., 2015) have shown promising results to retrieve stand and canopy forest attributes, including tropical forest AGB with no sign of saturation (e.g. Bastin et al., 2014; Ploton et al., 2012). Generally speaking, texture analysis (sensu Haralick, 1979) gives us a measure of the spatial arrangement of grey levels within a canopy image by directly reflecting the contrasts between sunlit and shadowed surfaces, thus providing information on the size and distribution of crowns of canopy trees and inter-crown canopy gaps. Texture is scale-dependent, so that meaningful texture metrics have to be multi-scale by nature or at least measurable at multiple spatial scales. In the Fourier Transform Textural Ordination (FOTO) method (Couteron, 2002; Proisy et al., 2007), texture analysis is carried out within unit-windows large enough (e.g. of c. 1 ha or more) to capture pseudo-periodic repetitions of the patterns of interest, that is local variations in crown and gap sizes. On each unit window, the Fourier transform is applied on the 2D autocovariance function of the grey levels which intrinsically conveys multiscale information. The resulting Fourier spectrum describes the dominating scales of grey levels variation within the unit window. In a second step, Fourier spectra extracted from a large number of unit-windows covering a large forest tract (e.g. hundreds of square kilometers or more), are systematically compared using standard multivariate ordination techniques such as Principal Component Analysis, thus displaying the unit-windows along uncorrelated texture gradients that facilitate their separation and interpretation. Texture indices (i.e. unit-window scores on the main PCA axes) are then used as independent variables in a regression analysis summarizing the statistical relationship between canopy texture and stand structure parameters, for instance AGB, as measured from field plot data (e.g. Couteron et al., 2005; Proisy et al., 2007). The basic idea is that once calibrated, such relationships can be used to predict and map stand structure parameters outside the sampling plots, directly from texture analysis of a canopy image (Fig. 1).

To date, the FOTO method has been applied in a number of tropical forest case studies to derive plot-level AGB estimates (e.g. Ploton et al., 2012; Proisy et al., 2007; Singh et al., 2014). Study areas generally covered a few hundreds of square kilometers, corresponding to one or two VHSR images. At such a scale the texture gradient provides good relationships with forest stand structure parameters, with a relative error on 1-ha plot AGB estimations generally below 20%. It has indeed been demonstrated from simulations that in closed-canopy forests, FOTO-texture indices characterize the size distribution of canopy crowns (Barbier et al., 2012), which are allometrically linked to tree size and AGB (Jucker et al., 2017; Ploton et al., 2016). However, it is increasingly evident that the texture-structure relationship is forest type- and/or site-dependent (Bastin et al., 2014), thus limiting broad-scale applications. As a consequence, mapping forest AGB on large mixed-forest landscapes currently requires a stratification into homogeneous texture-AGB strata (e.g. Bastin et al., 2014). It is worth mentioning that similar limitations are encountered when mapping forest AGB with airborne LiDAR data, requiring complementary information layers to allow multi-site comparisons (e.g. Asner et al., 2011; Vincent et al., 2014, 2012). Much like the universal airborne LiDAR approach (Asner et al., 2011), generalizing the texture-structure relationship

across contrasted forest types from different regions of the world would be a major step toward an operational method to monitor forest structure and AGB from VHSR optical data. This paper is a first attempt in this direction, which tries to overcome two major limitations of the current FOTO approach.

The first limitation is that in a VHSR canopy image, tree crowns and gaps are visible to the naked-eye from local brightness variations, but texture patterns captured by FOTO cannot discriminate large tree crowns from canopy gaps as they both appear as aggregates of bright or dark pixels of similar size in the image. Coarse FOTO-texture thus indistinctly results from either closed canopies comprising large tree crowns or from open canopies where aggregates of tree crowns alternate with canopy openings. Thus, a same FOTO-texture may represent high or low AGB values, respectively (see for instance, Pargal et al., 2017). Our hypothesis is that environmental conditions and type of gap dynamics influence canopy structure and heterogeneity, and in turn makes texture-structure relationships vary across sites. To overcome this drawback, we sought to complement FOTO texture with additional texture features characterizing other aspects of the canopy structure. We focused in particular on lacunarity analysis and derived texture features, which provides a quantitative measure of image ‘gapiness’ and proved to correlate well with canopy cover and gap volume on simulated forest stands (Frazer et al., 2005).

A second major constraint limiting the empirical exploration of the link between canopy texture and the underlying forest stand structure over large regions covered by several VHSR images is of instrumental nature. Forest texture indices are indeed sensitive to sensor optical properties and spatial resolution (Ploton et al., 2012; Proisy et al., 2007), but also to sun-sensor geometry (Barbier et al., 2011; Barbier and Couteron, 2015). Disentangling the effects of forest structure and instrumental configuration on canopy texture requires having a sufficiently large set of VHSR images acquired in controlled sun-sensor configurations and covering an extensive network of ground-truth field plots of varying stand structure and canopy aspect. An efficient workaround is to adopt a modelling approach coupling the simulation of spatially explicit 3D forest stand models (referred to as “mockups”) and the generation of virtual canopy images by applying a radiative transfer model onto the 3D mockups (Barbier et al., 2012). By controlling parameters of the radiative transfer model, canopy images in identical acquisition configurations can be generated for a variety of 3D stand mockups. Building forest mockups from simple tree shapes and stand inventory data (e.g. tree diameter distributions, local tree size allometries) may appear as a coarse representation of reality, but it is sufficient to capture how the 3D arrangement of stems and leaves interacts with important processes of the forest dynamics (Stark et al., 2015; Taubert et al., 2015). The simulation approach proved a valuable tool to bridge the gap between ground observations and remote sensing data (e.g. Frazer et al., 2005; Schneider et al., 2014), and ultimately help us understand how signal information can be reliably interpreted in terms of biophysical parameters.

In this study, we used a simulation approach based on extensive field inventory data to test whether a generalized canopy texture model could provide consistent estimates of AGB across structurally contrasted forest types. We first generated virtual canopy scenes in homogeneous acquisition configurations from 279 1-ha field plots collected in several tropical forest sites on three continents. These virtual canopy scenes allowed us to address how canopy texture features in contrasted forest dynamics and environmental conditions vary with the underlying stand structure, notably AGB. More specifically, we investigated from these simulated images the respective merits of the FOTO method and the lacunarity analysis in predicting AGB both locally (within sites) and globally (across sites), and explored whether combining the two methods improved AGB prediction models. Finally, we tested the texture-structure inversion model developed from simulations on three real Pleiades images acquired in comparable configurations over 49 1-ha field plots from a complex mosaic of forest types in Central Africa.

2. Material and methods

2.1. Forest inventory data

As a basis of both empirical estimations of forest plot AGB and simulations of 3D stand mockups for generating virtual canopy images, we used inventory data from a set of 279 1-ha forest sample plots in tropical Africa (157 ha), India (37 ha), and French Guiana (85 ha). Forest inventory data contained tree diameter at breast height (D) for all trees with $D \geq 10$ cm, for a total of 142,791 trees. Tree taxonomic identification was available at the species level for 78% of the trees, at the genus level for 6%, at the family level for 5% and 11% of the trees were left unidentified. We used the Dryad Global Wood Density Database (Chave et al., 2009; Zanne et al., 2009) and the World Agroforestry Center's Wood Density Database (ICRAF, 2007) to attribute to each individual tree the mean wood density value of its species. For those known only to the genus or family level, the average wood density at that taxonomic level was used (Chave et al., 2006). Unidentified individuals were attributed the average wood density of the 1-ha plot. Besides D , other tree dimensions were recorded on a subset of trees per plot, namely total tree height (H , $n = 23,237$), trunk height (H_t , $n = 6502$) defined as the height to the lowest main living branch (as in Ploton et al., 2016, see also interactive discussion on this paper for more information) and tree crown diameter (Cd , $n = 4438$). The distribution of field inventory data among sampling sites is provided in Table A1. We established allometric models for tree H , H_t and Cd in order to predict the dimensions of unmeasured trees. In each plot, we used allometric models established at the plot-, site- or regional-levels (i.e. Africa, India and French Guiana) depending on data availability.

Following Feldpausch et al. (2012), we used a three-parameter Weibull function to predict tree H from D : $H = a(1 - \exp(-bD^c))$. Trunk height was modeled as a power function of H : $H_t = a^*H^b$, fitted in logarithmic units and accounting for Baskerville correction (Baskerville, 1972). The same model and transformation were applied to fit the crown diameter, Cd , to D , at the exception that a 2-segments model was used when a significant breaking point was found in the relationship (following the procedure described in Antin et al., 2013). Finally, we used the pantropical model of Chave et al. (2014), including D , H and wood density to compute tree AGB estimates. In order to avoid increasing technical complexity, errors on AGB estimates from field data were neglected in this paper, though they would have to be accounted for and propagated through the up-scaling process in operational applications (e.g. Pargal et al., 2017; Réjou-Méchain et al., 2017).

Overall, the sample plots spanned wide gradients of tree density (139 to 848 trees ha^{-1}), stand basal area (10.3 to 57.7 $\text{m}^2 \text{ha}^{-1}$) and dominant height (17.8 to 50.5 m), and thus captured a large array of forest age and 3D organizations.

2.2. Generation of 3D forest mockups

In order to simulate, using a radiative transfer model, realistic virtual canopy images in homogenous acquisition configurations, we constructed 3D representations of the 279 1-ha sample plots using local tree allometries and tree location data (either exact coordinates or by sub-quadrats of 20 m sides). The 3D modelling procedure of a sample plot can be summarized as follows: (1) we built a simplified representation of each tree in the plot with the crown modeled as an ellipsoid of diameter Cd and depth H_c (i.e. $H - H_t$, in m) using field measurements if available or local allometric models otherwise; (2) if tree coordinates within the plot were known (i.e. for 135 of the 279 1-ha plots), we generated a single plot mockup by placing trees at their actual position; if tree positions were only known at the quadrat-level (i.e. for the remaining 144 plots): (i) trees were sorted from the tallest to the smallest; (ii) starting from the tallest tree downward, trees were tentatively located in their respective quadrats by generating random X and Y coordinates within an uniform distribution, and; (iii) retained if

their crown volume did not overlap crowns of already placed trees by $> 25\%$ of tree crown volume. If the algorithm failed to place a tree after 50 iterations (in 5.3% of the cases), its crown diameter was reduced by randomly sampling a value in the distribution of the crown diameter allometric model residuals. For those 144 plots, we generated 3 mockups per plot so as to capture some variability in canopy texture emerging from the random component of the mockup generation algorithm.

In order to help the interpretation of the canopy texture analyses introduced further in this paper, we also extracted from the 3D stand mockups simple parameters of stand structure and heterogeneity, such as mean and maximum tree sizes, stand gap fraction (defined as the cumulated area of pixels < 2 m in height) and canopy roughness (defined as within-plot variation of canopy height, Table 2).

2.3. Simulation of canopy images

We simulated very-high spatial resolution optical images of the 567 forest mockups using the Discrete Anisotropic Radiative Transfer model (DART, version 5.5.3, Gastellu-Etchegorry et al., 2015). DART is able to handle the forest mockups as a 3D array of cells (voxels) of different sizes. We used 1-m^3 voxels so to match with the metric resolution at which FOTO analyses are typically performed. Voxels contain a mixture of air and vegetation elements, either as solid facets or as turbid medium with a predefined distribution of leaf volume density. As leaf and bark optical properties of most tree species in our plots were not available, we used the optical properties of a single African canopy tree species (*Terminalia superba* Engl. & Diels) as input parameters for all the trees in DART. Tree trunks were represented as solid cylinders and crowns as turbid ellipsoids with a spherical distribution of leaf angles. Volume density within tree crown cells was adjusted to represent a realistic range of Leaf Area Index at the plot scale: (i) we computed the cumulated crowns volume of each plot; (ii) calibrated the vector of plot cumulated crowns volume to plot LAI by assigning a LAI of 4 and 8 to its 5th and 95th percentiles, respectively, and; (iii) used this relationship to derive the LAI of each plot and associated crown cell densities. Plot-scale LAI varied from 2.2 in the most open-canopy, low-density plots to 9.9 in the most highly packed plot (with mean \pm sd of 6.3 ± 1.4), in good agreement with tropical forest LAI estimations available in the literature (Asner and Martin, 2008; Vincent et al., 2017). To represent a vegetated understory in open canopy forests, we additionally attributed to the lowest 1-m layer above the ground the optical properties of a pioneer tree species (*Musanga cecropioides* R.Br. ex Tedlie) with a spherical distribution of leaf angles and leaf area density of $0.3 \text{ m}^2 \text{m}^{-3}$.

We used DART in ray tracing, reflectance mode with the sun and the atmosphere as the only radiation sources. We simulated top of atmosphere (TOA) panchromatic reflectance images (see Gastellu-Etchegorry et al., 2015 for further details) in the $0.35 \mu\text{m}$ – $1.1 \mu\text{m}$ domain that we decomposed into 75 spectral bands of $0.01 \mu\text{m}$ each. The radiative transfer calculations were conducted to represent viewing and solar illumination elevation angles set to 70° and 56.5° , respectively, and a solar-viewing azimuth difference set to -92° , to match the acquisition parameters of our real satellite images (see Section 2.4). For each DART image pixel, the reflectance channel of any VHSR sensor can then be obtained from the convolution of reflectance values provided in the 75 bands by the sensor's modulation transfer function. Computation time was about 40 min per image with about 12 GB of RAM on 64-bit Windows with an Intel Core i7 GHz processor.

2.4. Real satellite images

To test on real VHSR optical images the texture-structure inversion models developed with the simulated canopy images, we used a set of three Pleiades images acquired over a network of 49 1-ha sample plots in the transition area between evergreen and semi-deciduous forests of

Eastern Cameroon, in central Africa. Images were taken approximately two years after the establishment of the sample plots. Although the three images were in backward configuration (i.e. with sun behind the sensor), textural bias between images induced by image acquisition configurations is expected to be low thanks to fairly homogeneous acquisition angles (Table 1; Barbier and Couteron, 2015). Following previous applications, texture analysis was based on panchromatic band (450–830 nm) images, resampled from 0.7 m to 1 m per pixel through mean pixel aggregation.

2.5. Extraction of texture features from real or simulated canopy images

We performed texture analysis of panchromatic VHSR canopy images using both FOTO (Couteron, 2002) and lacunarity (Frazer et al., 2005) analyses as they are expected to provide complementary information on stand structure attributes. FOTO method has been extensively described elsewhere (e.g. Couteron, 2002; Couteron et al., 2005) and we only give a brief outline of the procedure hereafter. The first step consisted in dividing a panchromatic satellite image into square 1-ha unit canopy windows (with 1-m spatial resolution thus a spacing of $S = 100$ in both X and Y directions), a size which proved suitable from previous studies to capture several repetitions of the largest tree crowns in closed forest stands (Couteron, 2002; Proisy et al., 2007). On each unit-window, the two-dimensional Fast Fourier Transform (fft2) function was applied to transpose the spectral radiance from the spatial domain to the frequency domain, using sine-cosine functions at integer frequencies (i.e. wavenumbers, 1, 2, ..., $S/2$) along the X and Y directions of the plane. The squared amplitude of the fft2 yields a 2D periodogram, which represents an apportionment of the variance in spectral radiance among spatial frequency bins in all possible planar directions within the unit canopy window. The orientation information was here neglected by averaging the periodogram across directions, which provided the one-dimensional so-called radial- or r-spectrum. Knowing image spatial resolution (1 m), wavenumbers can equivalently be expressed in wavelengths (λ , in m) so that a r-spectrum gives the frequency distribution of the number of times a pattern of size λ repeats itself in a 1-ha unit canopy window. A characteristic of the method is that sampling according to harmonic Fourier frequencies (stemming from fft2) results in denser spectrum values as λ decreases, so that intermediate scales of patterns relevant for canopy characterization may be poorly sampled. To overcome this we used the modified algorithm presented in Barbier and Couteron (2015), in which, after signal centering, unit-window size is doubled in each direction using zero-padding (Cressie, 1993), which allows increasing intermediate λ sampling. The resulting list of λ was pruned to conserve a sampling of λ values as regular as possible, thus decreasing information redundancy at small wavelengths. Finally, a set of 25 λ values was retained from 2 up to 99 m. All r-spectra were assembled into a single table, F, with the individual 1-ha unit-windows as rows and Fourier spatial frequencies as columns. Unit-windows with r-spectra dominated by high Fourier frequencies (low λ) are expected to display fine grain canopy textures due to the succession of small tree crowns, while coarse grain canopy textures correspond to r-spectra dominated by low Fourier frequencies expected to reflect the repetition of large canopy trees (see e.g. Barbier et al., 2012).

Lacunarity was formally defined by Mandelbrot (1983) as the deviation of a fractal pattern from translational invariance, a concept further expanded to non-fractal patterns (Allain and Cloitre, 1991). It basically measures how patterns fill space, those having more or larger gaps having generally a higher lacunarity or gapiness. In the present paper, we computed lacunarity following Frazer et al. (2005) to which the reader should refer for more details. Lacunarity was computed in the same 1-ha unit canopy windows as Fourier r-spectra. On each unit-window, a moving square box of size s (in pixels) is glided by one pixel at a time along all rows and columns. For each box of size s , the mass, M , is computed as the sum of all pixel spectral radiance (previously

normalized per unit-window), so that the probability distribution function $Q(M, s)$ represents the frequency distribution of M divided by the number of boxes at size s . The lacunarity statistic is then computed as $\Delta(s) = Z_Q^{(2)}(s)/(Z_Q^{(1)}(s))^2$, where $Z_Q^{(1)}(s)$ and $Z_Q^{(2)}(s)$ are the mean and mean of squared values of $Q(M, s)$, respectively. In our study we used 10 discrete box sizes, s , from 1 to 99 m, and normalized all lacunarity values per unit canopy windows by dividing them by $\Delta(1)$. We then denote as a lacunarity spectrum the series of normalized lacunarity statistics computed at each box size for a given unit-window. All normalized lacunarity spectra for a given satellite image were assembled into a single table, L, with the unit-windows as rows and the box sizes as columns. The decreasing pattern of lacunarity with increasing box size reflects the rate of increase in canopy heterogeneity from the finer to the coarser scale patterns, which in the context of forest canopies is related to the degree of inter-crowns canopy openness (see Frazer et al., 2005).

2.6. Statistical analyses

2.6.1. Canopy texture indices

In order to systematically compare unit-windows textural properties (as characterized by Fourier and lacunarity spectra), both the F and L tables were submitted independently to Principal Component Analysis (PCA) as in Couteron et al. (2005) and Frazer et al. (2005). The F and L tables were column-wise normalized prior to perform PCAs, which allows uncovering texture gradients even when the absolute variation between unit-windows is small. This led to two independent sets of texture gradients, synthesizing FOTO-texture indices on the one hand (that is, unit-windows scores along the axes of the PCA on the F table, or F-PCA) and Lacunarity-texture indices on the other hand (i.e. unit-windows scores along the axes of L-PCA). We then investigated the agreement between these two analyses using a co-inertia analysis (COIA; Dolédec and Chessel, 1994; Dray et al., 2003). COIA is a simple and robust method for the simultaneous analysis of two data tables matching by observations (here, unit canopy windows). The method maximizes the square covariance between the projected coordinates of the unit-windows on the PCA axes of F and L. It thus simultaneously maximizes the variance in F and L separately (the two PCAs) and the correlation between the two sets of principal components. The texture gradients captured by FOTO and by the lacunarity analysis can thus be projected on common orthogonal components. The unit-window scores on these components are canopy texture indices used in further analyses as image-derived predictors of plot-level AGB.

2.6.2. Modelling global and local texture – AGB relationships

We used the Random Forest (RF) algorithm as implemented in the package “randomForest” version 4.6.12 of R statistical software (R Core Team, 2016) to develop global (i.e. across sites) forest AGB regression models based on canopy texture indices. RF is an ensemble of learning methods for classification and regression based on decision trees (Breiman, 2001) increasingly used in remote-sensing studies, notably for carbon mapping (Baccini et al., 2012; Mascaró et al., 2014; Vieilledent et al., 2016). The aim is to overcome over-fitting problems

Table 1

Date and acquisition parameters of Pleiades panchromatic satellite images over Eastern Cameroun, Central Africa.

Date		Sensor		Sun	
Month	Year	Azimuth	Elevation	Azimuth	Elevation
12	2014	227.6	64.5	145.3	57.0
12	2014	248.5	79.7	146.4	55.3
1	2015	229.6	65.7	138.3	57.3

#1 catalog ID: DS_PHR1A_201412210944201_FR1_PX_E013N03_0909_01764.

#2 catalog ID: DS_PHR1A_201412210943258_FR1_PX_E013N05_0606_01395.

#3 catalog ID: DS_PHR1A_201501160944349_FR1_PX_E013N03_0702_00899.

that can occur using individual decision trees. The algorithm builds a large number of decision trees that are trained on random samples of both the training set (i.e. the observations) and the predictor variables, and outputs the average of individual trees predictions. An interesting feature of such machine learning techniques is that it allows integrating a large number of variables of potentially different statistical distributions (Marvin et al., 2016) and does not require specifying an explicit

model form.

We used a similar (RF) regression framework, but with forest “site” taken as a random variable in regression models, to assess the predictive power of canopy texture indices on plot AGB at the local level (i.e. within sites). The mixed-effects RF model (MERF, Hajjem et al., 2014) is defined as a classical linear mixed-effects model (Wu and Zhang, 2006), except that a more general and unknown function, $f(X_i)$,

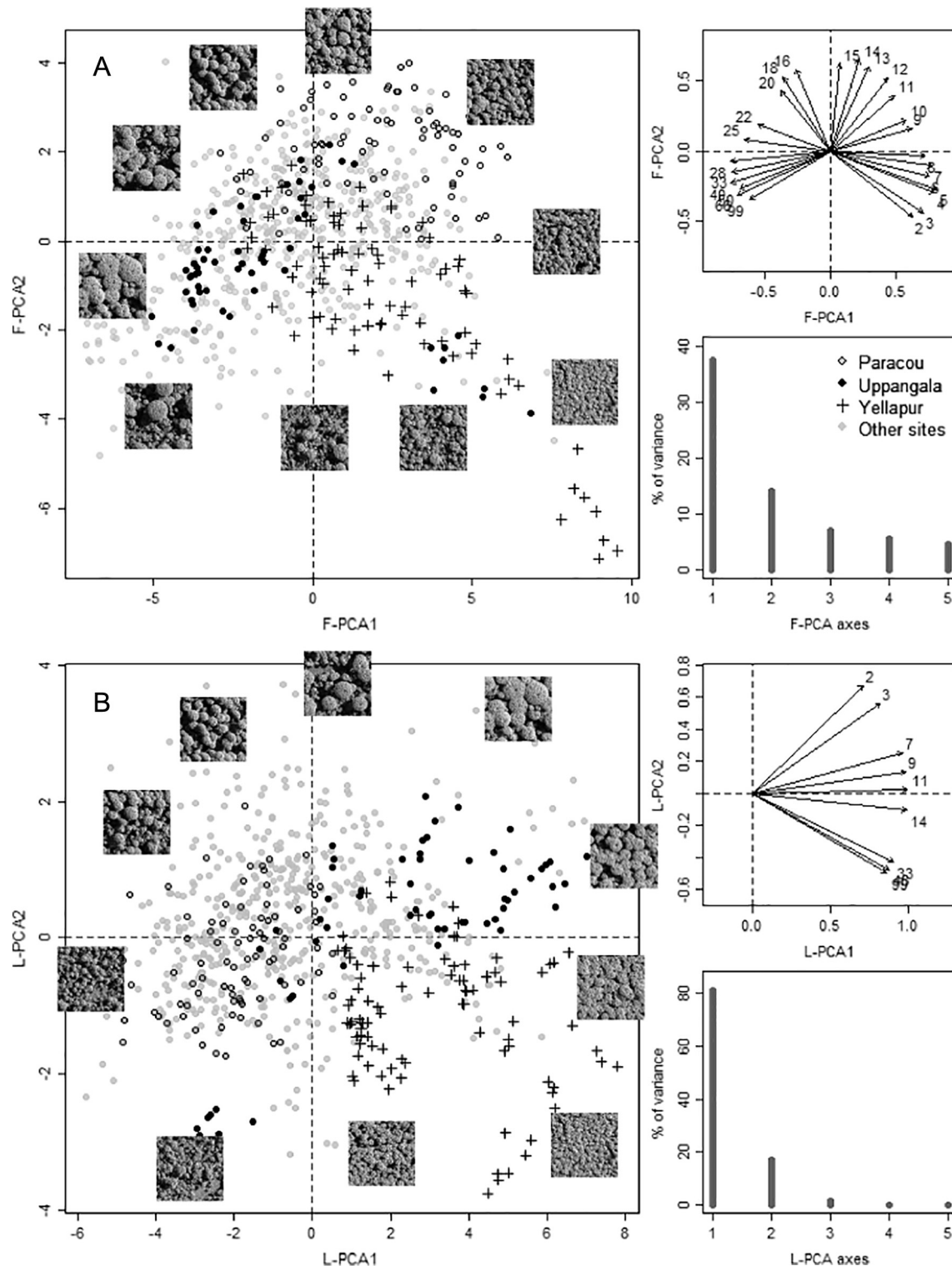


Fig. 2. Canopy texture ordinations based on (A) the FOTO method and (B) the lacunarity analysis. In both cases, scatter plots of PCA scores along the first two principal axes are shown (left panels), with 3 example sites highlighted with particular symbols (Paracou, Uppangala and Yellapur). Top-right panels represent correlation circles with wavelength, λ (A) or box size, s (B) in meter. Bottom-right panels represent histograms of Eigenvalues in % of total variance.

where i denotes a forest site, is used to estimate the within-site fixed effect using RF in place of the usual linear predictor, the random part of the model being still assumed linear. The model is fitted with an expectation-maximization (EM) algorithm (see Hajjem et al., 2014 for details and R script). For simplicity, across site variations in texture – AGB relationships were accounted for with site-specific random intercepts only.

2.6.3. AGB models validation

We evaluated regression model errors using a five-fold cross-validation procedure independent of the internal validation scheme of RF. The dataset was randomly split into 5 folds of approximately equal size and the AGB of forest plots in each fold was predicted with the regression model calibrated on the four other folds. This procedure was repeated 10 times so to compute mean and standard deviation of goodness-of-fit statistics. For each model, we report the amount of variation explained as computed from calibration (R^2_c) and validation (R^2_v) data. Using validation data only, we further provide the root-mean-square error (RMSE) and relative RMSE (rRMSE in %), along with the mean signed deviation (MSD), used to compare site-level prediction bias in RF and MERF models (Xu et al., 2016).

3. Results

3.1. Texture analysis of virtual canopy images

We applied both the FOTO method and the lacunarity analysis on all unit canopy windows simulated from the 279 1-ha plots of tropical forest inventory. The first factorial plane of FOTO-PCA explained 51.1% (37.2% and 13.9% for axes 1 and 2, respectively) of the total variability among Fourier r-spectra (F-table) and produced a typical correlation circle with spatial patterns sorted from short to long wavelengths (or from high to low frequency/wavenumber) (Fig. 2A). Wavelengths (λ) of about 5 to 10 m (visually relating to small crown sizes) were found on the positive side of the first PCA axis (F-PCA1), intermediate λ (15 to 20 m) on the positive side of F-PCA2 and λ of 25 to 35 m (largest crown sizes) on the negative side of F-PCA1. The ordination gradient on the first FOTO-PCA plane thus corresponded to a fineness-coarseness canopy texture gradient, with aperiodic canopies found close to the origin and heterogeneous ones (i.e. mixing small and large crown patches) found on the lower-left part of the plane. The general decrease of canopy grain size along F-PCA1 negatively correlated with stand maximum tree size (Pearson's $r \approx -0.7$ with DBH_m and H_m in Table 2) and canopy roughness ($r = -0.65$ with H_v10), which coincided with a moderate decrease of parameters reflecting stand aggradation ($r = -0.48$ and -0.42 with DBH_{mean} and G , respectively).

The first Lacunarity-PCA plane explained 98.1% (81.2% and 17% for axes 1 and 2, respectively) of the variance among normalized lacunarity spectra (L-table). The first PCA axis (L-PCA1) sorted unit-windows according to their degree of gapiness (Fig. 2B) as shown by a negative correlation with stand gap fraction ($r = -0.57$ with GF in

Table 2), which coincided with a positive correlation with stand basal area ($r = 0.6$) and mean tree diameter ($r = 0.48$). L-PCA1 thus sorted unit-windows from fairly open stands (featuring frequent patches of small trees, < 2 m in height) to fully-stocked stands having a canopy made of larger trees. L-PCA2 captured variations in the rate of decrease in lacunarity with box size, which reflected a gradient in canopy grain and heterogeneity. Fairly homogeneous canopy (smooth canopy grain) characterized by a low rate of decrease in lacunarity with box size were found on the negative side of L-PCA2, while heterogeneous canopy were found on the positive side of L-PCA2. As a matter of fact, L-PCA2 was positively correlated with the canopy roughness index, H_v10 ($r = 0.61$) and with maximum tree size ($r = 0.76$ and 0.66 with H_m and DBH_m , respectively). F-PCA1 and L-PCA2 displayed a very high correlation of 0.93 (axes orientations are arbitrary and not informative in PCA) and fundamentally depicted the same coarseness – fineness gradient of canopy aspect. On the other hand, correlations between F-PCA2 and both Lacunarity-based PCA axes were weak, suggesting complementarity.

Combining the F and L tables in a common co-inertia analysis (Fig. 3) confirmed a slight but significant co-structure, with a RV coefficient (equivalent to the R^2 between two variables) of 0.27 ($P < 0.001$). The first COIA plane captured 99% of the co-inertia, which was mostly one-dimensional (61.9% on COIA-1). The first COIA plane (i.e. COIA-1 and 2) also captured 91.5% and 98.6% of the cumulated inertia projected on the first F-PCA and L-PCA planes, respectively. Fig. 3 illustrates that while the co-inertia analysis preserves the structure of each separate PCA, i.e. the canopy texture gradients described by the FOTO (Fig. 3A) and lacunarity analyses (Fig. 3D), some disagreements between the two methods appeared at both the site and unit-window level. On the first COIA axis (COIA-1) for instance, Yellapur and Paracou sites are very close to each other and far from Uppangala in terms of mean FOTO-texture properties (large empty circles in Fig. 3C), while Yellapur is intermediate between Paracou and Uppangala in terms of mean lacunarity-texture properties (large full circles, Fig. 3C). In Paracou, canopy texture described by FOTO and lacunarity provided very similar information for all the unit-windows (short arrows in Fig. 3F), while for Yellapur and Uppangala, some unit-windows that exhibited very different FOTO textures (i.e. found at the opposite on COIA-1) showed a convergence toward similar lacunarity-derived textures (long convergent arrows in Fig. 3F). This demonstrates that FOTO and Lacunarity texture gradients, although globally correlated, can combine differently at the scale of unit-windows, and thus bring relevant information for discriminating individual canopy features.

3.2. Canopy texture - AGB models

We built global stand AGB prediction models based on the two first axes of either F-PCA (F-model) or L-PCA (L-model) derived from the virtual canopy images (Fig. 4A, C). Both models provided quite low goodness of fit ($R^2_c = 0.20$ and 0.42 for F- and L-model, respectively).

Table 2

Correlation between stand structure parameters extracted from three-dimensional mockups and canopy window scores on the texture ordination axes based on the FOTO method (F-PCA1 and F-PCA2) and the lacunarity analysis (L-PCA1 and L-PCA2). Probability value of Pearson correlation test are provided between brackets and coded following standard notation (***) $P \leq 0.001$, ** $P \leq 0.01$, * $P \leq 0.05$, ns = non-significant).

Stand structure parameters		F-PCA1	F-PCA2	L-PCA1	L-PCA2
GF	Gap fraction (cumulated area of pixels < 2 m in height)	− 0.04 (ns)	0.15 (***)	− 0.57 (***)	0.07 (*)
H_v10	Standard deviation of maximum tree height among 10 m quadrats	− 0.65 (***)	− 0.24 (***)	− 0.24 (***)	0.61 (***)
DBH_m	Stand maximum tree DBH	− 0.69 (***)	− 0.21 (***)	0.23 (***)	0.66 (***)
H_m	Stand maximum tree height	− 0.71 (***)	0.1 (**)	− 0.12 (**)	0.76 (***)
Cd_m	Stand maximum crown diameter	− 0.56 (***)	− 0.2 (***)	0.28 (***)	0.53 (***)
N	Stand tree density	0.2 (***)	0.1 (**)	− 0.01 (ns)	− 0.12 (**)
G	Stand basal area	− 0.42 (***)	0.06 (ns)	0.6 (***)	0.44 (***)
DBH_{mean}	Quadratic mean of tree DBH	− 0.48 (***)	0 (ns)	0.48 (***)	0.43 (***)
CD_{mean}	Quadratic mean of tree crown diameters	− 0.29 (***)	− 0.08 (*)	0.45 (***)	0.22 (***)

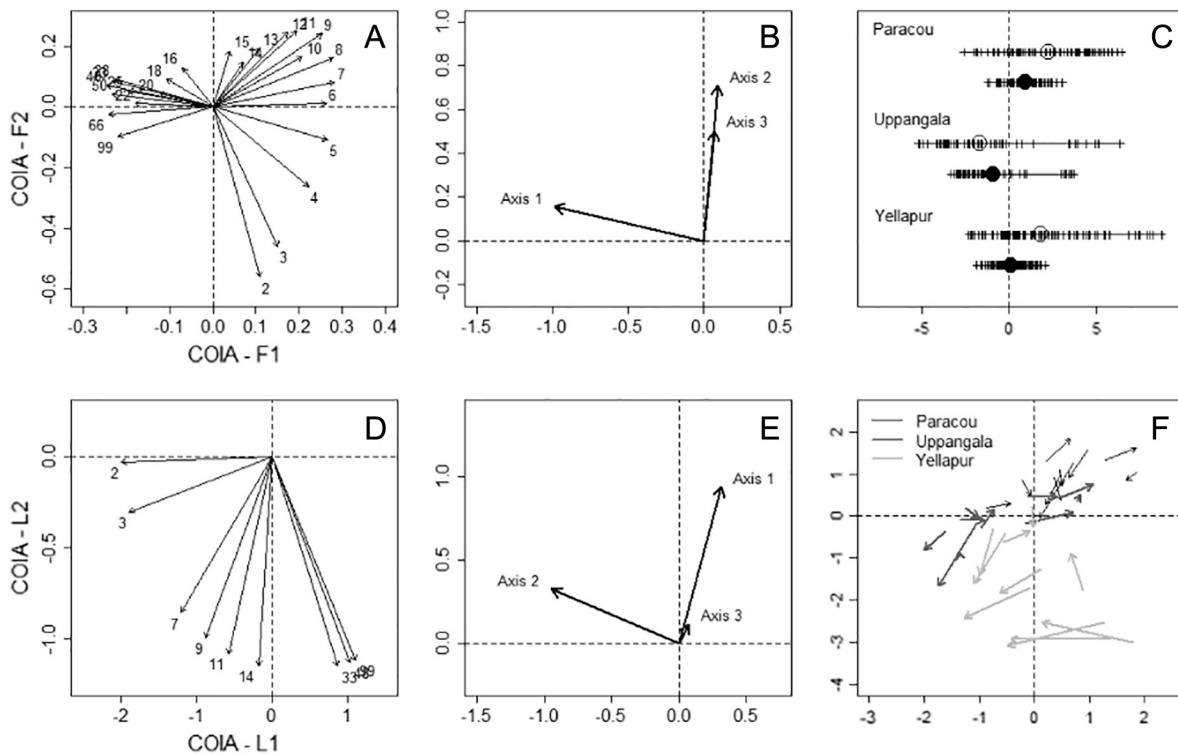


Fig. 3. Co-inertia analysis. Position on the first co-inertia plane of the FOTO r -spectra wavelengths, λ (A) and the lacunarity box size, s (D). Components of the F-PCA (B) and the L-PCA (E) projected onto the co-inertia axes. Ordination of windows from the 3 example sites (Paracou, Uppangala and Yellapur) on COIA-1 (C) with large empty and full circles representing the average site-level score for FOTO and lacunarity features, respectively. Normed scores of 10 randomly sampled canopy windows from the 3 example sites on the first co-inertia plane (F), with each arrow linking a unit-window position for FOTO and lacunarity characteristics, respectively.

Model R^2 computed from independent validation data were even lower ($R^2_v = 0.09$ and 0.31), indicating that the internal validation scheme of RF tends to overestimate model performance. The two models showed a general bias with respect to the 1:1 line, with a tendency to overestimate low biomass levels and underestimate high biomass levels, as well as more or less pronounced positive or negative biases occurring at the site-level (up to $MSD = -32\%$ for the L-model at Paracou). Using a mixed-effect RF algorithm (MERF) with a random site effect largely improved goodness-of-fit statistics ($R^2_v = 0.31$ and 0.61 for F- and L-model, respectively, Fig. 4B, D), indicating that a substantial gain in AGB prediction can be achieved when accounting for local (i.e. site-level) variation in texture – AGB relationships.

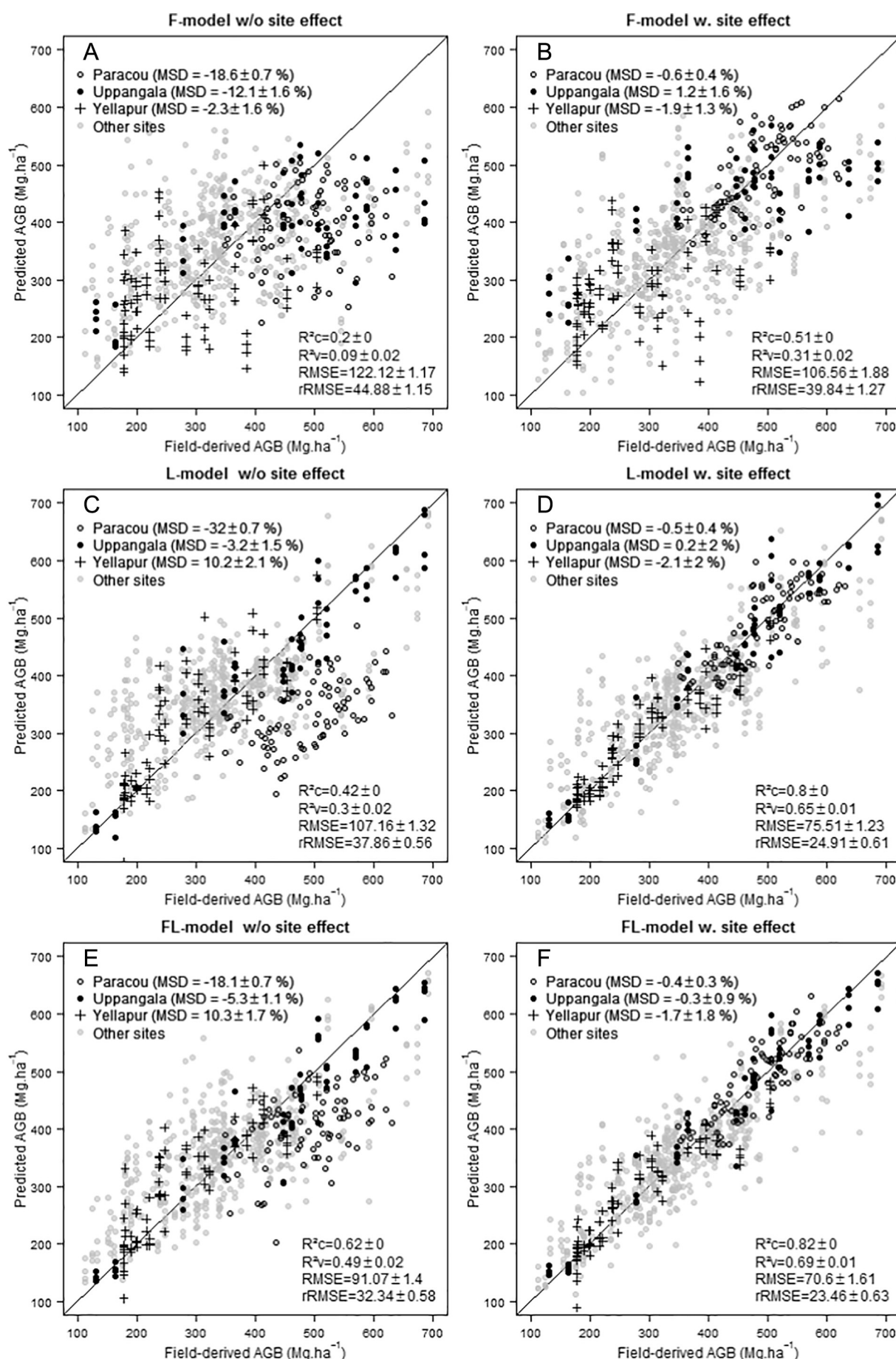
Combining both FOTO and Lacunarity texture features from COIA in a single global model (FL-model in Fig. 4E) increased the prediction power on stand AGB ($R^2_v = 0.49$ with $rRMSE = 32.3\%$). This global model also improved the prediction accuracy at Paracou ($MSD = -18.1\%$, Fig. 4E), but site-level MSDs remained substantial. It is noteworthy that site-level MSDs seemed to decrease with the range of biomass encompassed across plots in a site: while plots in Yellapur ($MSD = 10.3\%$) and Paracou ($MSD = -18.1\%$) are restricted to low and high biomass levels, respectively, in Uppangala ($MSD = -5.3\%$) plots have been sampled along a biomass gradient spanning from c. 150 up to $> 600 \text{ Mg ha}^{-1}$. This indicates that the underlying texture-AGB relationship varies across sites as a function of sampling, but it may also vary with respect to local site characteristics. For instance, while tree density in Paracou correlated well with FOTO and lacunarity scores on COIA-1 ($r = 0.74$ and 0.63 , respectively), it did not in Yellapur ($r < 0.18$). Similar observations can be made for maximum tree slenderness (i.e. H_m/D_m) which correlated well with scores in Uppangala ($r = 0.91$ and 0.88 , respectively) but not so clearly in Yellapur ($r = 0.42$ and 0.53 , respectively). Again, accounting for across site variation in the texture – structure model by including a random site effect largely improved model performance (Fig. 4F). The MERF FL-

model outperformed all other models, with $R^2_v = 0.69$ and $rRMSE = 23.5\%$.

Although the mixed modelling strategy proved powerful at sampled sites (i.e. where sample plots are available to account for a random site effect), it is not relevant to predict plot AGB in an unsampled new site. We therefore introduced in the FL-model a bioclimatic proxy, E , proposed by Chave et al. (2014), which is a compound variable based on water deficit, temperature and precipitation seasonality available as a global gridded layer at 2.5 arc sec resolution (see http://chave.ups-tlse.fr/pantropical_allometry.htm). E can be seen as expressing a bioclimatic stress on forest growth and was demonstrated to capture pantropical variation in forest AGB through its effect on tree height-diameter allometries (Chave et al., 2014), a source of variation than can hardly be captured by canopy texture. Fig. 5A shows indeed that E largely captured the random site effect of the FL-model, with a downward adjustment of plot AGB (i.e. negative random intercept) at sites with high bioclimatic stress (i.e. when E is positive and high) and vice versa. Incorporating E along with FOTO and lacunarity texture features (FLE-model, Fig. 5B) provided very similar results to the MERF FL-model ($R^2_v = 0.69$, with $rRMSE = 24.9\%$) while maintaining local prediction errors (MSD) of the 3 example sites below 10%.

3.3. Application to real satellite images

As the virtual canopy scenes are necessarily imperfect representations of canopy images, we also tested the texture – AGB models on a set of three real VHSR optical images acquired in homogeneous acquisition configurations over our sampling plots in central Africa. The F- and L-models did not, or weakly discriminate AGB variations ($R^2 = 0.08$ and $R^2 = 0.1$, respectively) among the 49 1-ha forest inventory plots. Combining F and L texture features (FL-model) led to a significant improvement of model goodness-of-fit ($R^2_v = 0.42$ with $rRMSE = 25.1\%$), which further improved by the inclusion of E as an



(caption on next page)

Fig. 4. Aboveground biomass prediction models based on FOTO texture (F-model), lacunarity texture (L-model) and the two sources of texture information (FL-model), either without site effect (RF algorithm, panels A, C and E) or with site effect (MERF algorithm, panels B, D and F). Texture features were extracted from virtual canopy scenes. Goodness of fit statistics are defined in the [Methods](#).

additional predictor (FLE model, $R^2_v = 0.46$ with $rRMSE = 23.2\%$, Fig. 6). Though a limited sample of canopy images in homogeneous acquisition configurations were available to us, these results from central Africa confirm the power of the FLE model to predict regional variation in plot AGB from real canopy images too.

4. Discussion

Over the past decade, about two dozen studies successfully used canopy texture analysis applied on VHSR optical or LiDAR canopy height models data to uncover spatial gradients of forest structure and AGB, including in high-biomass tropical forests (e.g. [Couteron et al., 2005](#); [Frazer et al., 2005](#); [Malhi and Román-Cuesta, 2008](#); [Proisy et al., 2007](#)). These studies were however limited to relatively small geographical areas and often retrieved structure gradients within a single, homogeneous forest type and image. The few attempts made in mosaics of heterogeneous forest patches (e.g. [Bastin et al., 2014](#); [Pargal et al., 2017](#); [Singh et al., 2014](#)) have shown that the link between canopy texture and stand structure depends on forest type, hindering broad-scale applications of texture-based methods. Using 279 1-ha plots distributed among different forest types across the tropics, we evaluated whether a generalized biomass prediction model based on canopy texture indices could provide consistent predictions at both local and global scales. The results presented here based on virtual canopy images show that it is worth complementing FOTO with lacunarity texture indices capturing canopy features related to canopy openness. Introducing a bioclimatic stress variable that captured regional variation in tree height-diameter allometry also substantially improved the accuracy and precision of forest AGB retrievals among forest sites. A practical application of the method to a mosaic of forest types in the Congo basin showed that forest AGB inferences could be made with reasonable precision (i.e. $\leq 25\%$ of error) up to 600 Mg ha^{-1} , without saturation.

4.1. Contrasted canopy texture - stand AGB relationships across sites

Global models based only on FOTO or lacunarity texture indices (F-

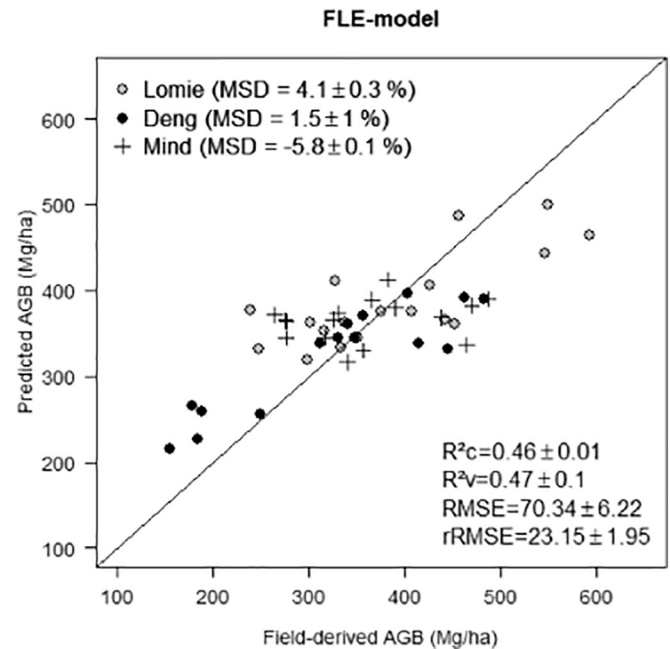


Fig. 6. Aboveground biomass prediction models based on FOTO texture, lacunarity texture and the bioclimatic stress proxy E (FLE-model). Texture features were extracted from three Pleiades covering 49 1-ha forest inventory plots in central Africa. Goodness of fit statistics are defined in [Methods](#) section.

and L-model, respectively) significantly explained AGB variations but presented a relatively high uncertainty ($rRMSE = 38\text{--}45\%$), consistent with what other studies have reported for heterogeneous forest landscapes (e.g. [Bastin et al., 2014](#)). To circumvent the problem and improve AGB inferences, previous empirical studies typically used a forest type stratification step prior to the calibration of within-class texture–AGB models, suggesting that the relationship is dependent on forest type ([Bastin et al., 2014](#); [Singh et al., 2014](#)). Our results indeed showed that forest plots from different geographical sites were often

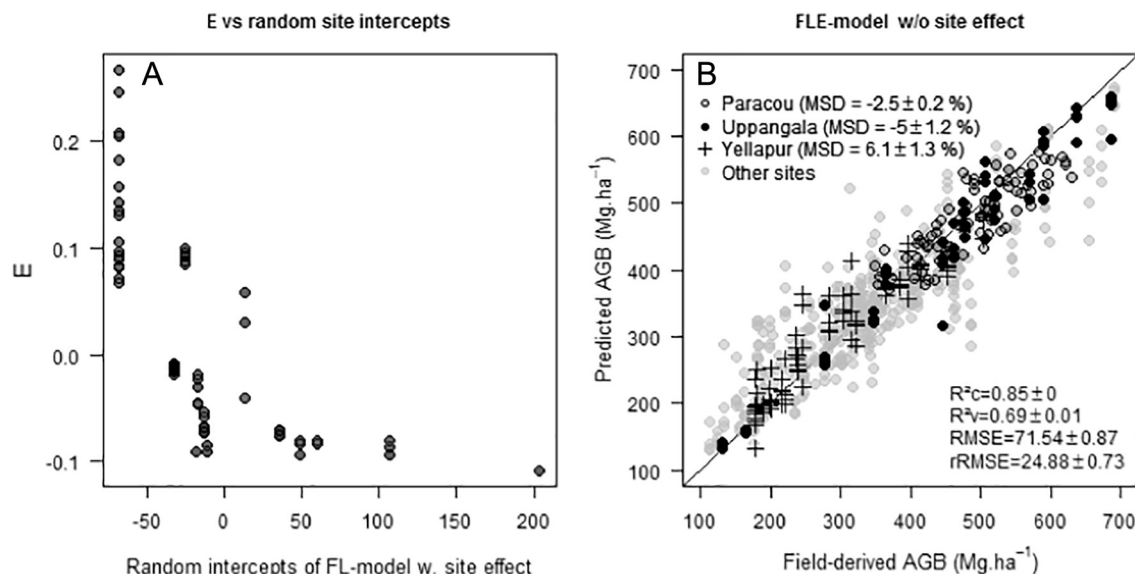


Fig. 5. (A) Bioclimatic proxy E vs random site intercepts of FL-model (in Fig. 4E); (B) Random forest AGB prediction model based on FOTO texture, lacunarity texture and E (FLE-model). Texture features were extracted from virtual canopy scenes. Goodness of fit statistics are defined in the [Methods](#).

clustered along the texture gradients and that texture indices did not always correlate with the same stand structure parameters at different sites, generating systematic biases in global models.

The relationship between FOTO-texture indices and forest AGB is expected to hold well for periodic canopy patterns with homogeneous grain size (Proisy et al., 2007). In this ideal case, Fourier r-spectra peak around the scale of the mean crown size of canopy trees (Barbier et al., 2010). Because crown size is allometrically related to tree AGB (Jucker et al., 2017; Ploton et al., 2016) and the AGB of the 20 biggest trees in 1-ha stands capture on average c. 85% of the variation across whole stands AGB (Bastin et al., 2015), FOTO texture accurately predicts variation in forest stand AGB. This is for instance the case along the successional development pathway of mangrove tree cohorts (Proisy et al., 2007) but can also apply to mixed-forests where the coarseness-fineness canopy texture gradient reflects differences in the stature of mature trees (e.g. due to contrasting soil fertility, Couteron et al., 2005) or along forest biomass gradients. At the Paracou study site for instance, a good linear correlation (Pearson's $r = -0.88$) existed between tree density (N) and the mean quadratic diameter (DBH_{mean}) suggesting that sample plots align along a self-thinning trajectory (see also Vincent et al., 2012). In this case, our simulation procedure based on simple allometric relationships thus produced fully-stocked mockups along with virtual canopy images often displaying a periodic aspect (see Fig. 2) and for which a local F-model (i.e. based on FOTO texture only) provided very accurate AGB predictions ($rRMSE = c. 10\%$). However, when the forest enters the gap phase dynamics (Withmore, 1975), stand structure becomes heterogeneous in both the horizontal and vertical dimensions, leading to higher canopy roughness, more frequent canopy gaps alternating with clusters of large trees (e.g. Franklin et al., 2002; Guariguata and Ostertag, 2001; Spies, 1998). In Uppangala for instance, where N and DBH_{mean} did not correlate over the sampling plots (Pearson's $r = -0.09$), simulated canopy images were highly heterogeneous (see Fig. 2), and a local L-model (i.e. based on lacunarity texture only) produced more accurate AGB predictions than a local F-model ($rRMSE < 10\%$ vs. c. 20%, respectively). Our study showed that lacunarity is an efficient method to reveal canopy openness and heterogeneity gradients, which confirms previous findings (e.g. Frazer et al., 2005; Malhi and Román-Cuesta, 2008) and stresses the importance of those canopy structural descriptors for predicting local variation of forest AGB at some sites (e.g. Uppangala). It is therefore easy to understand that, as hypothesized, complementing FOTO texture with lacunarity texture provided a more comprehensive description of the potential range of canopy structures and thus largely improved our multi-site prediction model (FL-model) at both the local and global levels.

At the global scale however, variation in canopy height (Fayad et al., 2016; Saatchi et al., 2011) and tree slenderness (Feldpausch et al., 2012), which proved critical for accurate AGB estimations (Chave et al., 2014), cannot be directly accounted for by a 2D analysis of canopy texture, whatever the method. Along a local forest successional gradient, canopy height variations follow increment in tree size visible from above through the mean crown sizes. But, the maximal height reachable by dominant trees is known to generally reveal the growth potential of a forest in relation to soil and regional bioclimatic constraints, in particular with regard to water stress (Chave et al., 2014). Introducing the E bioclimatic variable, which combines water deficit with temperature and precipitation seasonality (see Chave et al., 2014) improved goodness of fit of our global regression model (FLE-model) and significantly reduced local prediction errors. More studies are however needed to further test the robustness of the bioclimatic E variable as a proxy for forest potential height to be used in large-scale assessments of forest AGB from 2D optical data.

On the set of real images from the Congo basin, the generalized texture-based model was able to detect spatial variations in AGB within a tropical forest mosaic which may be seen as a difficult case since being characterized by both high AGB levels (i.e. average AGB over 49 field plots of $359 \pm 98 \text{ Mg ha}^{-1}$) and forest types showing important

variations in stand 3D structure, from closed-canopy mixed-species mature stands to open-canopy *Marantaceae* forests. We indeed found that the multi-site FLE-model was the most robust with uncertainty of about 70 Mg ha^{-1} at 1-ha scale ($rRMSE$) corresponding to a relative error of $< 25\%$ ($rRMSE$). This result confirms and expands the results previously obtained with a variety of satellite sensors (Quickbird, GeoEye, IKONOS, SPOT-5), aerial images and even images freely available from the Google Earth engine (Bastin et al., 2014; Meng et al., 2016; Ploton et al., 2012; Proisy et al., 2007; Singh et al., 2014, 2015) in temperate or tropical forests. This represents an important step toward using VHSR optical imagery for broad-scale assessments of forest AGB, as it eliminates the need of a preliminary forest classification (see for instance Pargal et al., 2017). Recent progress also opened the perspective to perform texture analysis on inter-calibrated satellite images from various sensors and/or in various configurations, provided they partly overlap (Barbier and Couteron, 2015).

4.2. On 3D stand mockups and virtual canopy images for model calibration

As canopy texture is sensitive to variation in shadowing pattern created by the various combinations of sun-sensor-scene angles (Barbier et al., 2011), we used in this paper a simulation approach to assemble a large array of above-plot VHSR canopy images in homogeneous acquisition configurations, which remains challenging from real satellite sensors. The approach based on 3D stand mockups derived from field data and allometric relationships, on which a radiative transfer simulation is applied, follows previously published studies on image texture simulations, notably Barbier et al. (2012, 2010), Barbier and Couteron (2015) and Proisy et al. (2016). At the scale of 1-ha forest plots, the size distribution of large objects (individual and aggregated tree crowns) and their spatial arrangements (e.g. inter-crown gaps and associated shadows, variations in tree density and size between subplots, etc.) determine the coarsest patterns visible on canopy scenes and are crucial determinants of spatial variations of the apparent reflectance. Using a unique, simplified tree shape representation (i.e. cylindrical trunks and non-plastic, ellipsoid crowns) allows generating sufficiently realistic brightness variation patterns at those coarse scales for the interpretation of canopy texture gradients. For instance, Proisy et al. (2016) showed that this approach allows producing texture r-spectra that have similar frequency peaks than the real image counterparts over a wide range of mangrove successional stages. In the present study, a particular care was taken to develop local tree size allometries and integrate field information on the spatial positions of trees within stands, so as to mimic the coarse-scale heterogeneity observed in real field plots. However, our stand simulation procedure could still be improved by accounting for crown shapes and plasticity (like for instance in Boudon and Le Moguédec, 2007) or for between-species variations in trees inner-crown properties, either geometric (e.g. foliage clumping and porosity, leaf angle distribution) or optical (Schneider et al., 2014), that may influence grayscale variations at smaller spatial scales. Considering these different aspects is a long term research effort, and will likely benefit from technological advances in LiDAR scanning and unmanned aerial vehicles (e.g. Morton and Cook, 2016). We suspect lacunarity analysis to be more sensitive than FOTO to these geometric and optical parameters, making lacunarity a complement to FOTO appearing more relevant when analyzing simulated images than when analyzing real images.

An invaluable advantage of virtual canopy images is that they can be simulated in homogeneous acquisition configurations on the basis of field data from different sites and regions. Texture indeed quantifies pattern characteristics related to the contrasts between sunlit and shadowed surfaces and is thus highly sensitive to the sun to sensor and scene angles (Barbier et al., 2011). Even if inter-calibration procedures can help, particular configurations (e.g. backward scattering modes, near hotspot directions) are intrinsically detrimental to canopy texture analysis and fatal to large-scale applications over a mosaic of several

images (Barbier and Couteron, 2015). Besides, programming image acquisition in controlled configurations, though possible, remains difficult, sometimes costly and often very long, particularly over tropical zones where optical images frequently suffer atmospheric pollutions related to dense cloud cover or persistent nebulosity. Another pitfall of the detection of texture gradients through ordination is that the principal axes extracted from the data are highly dependent on available samples and particular image sets may not reflect the entire possible gradients of forest structure and canopy texture variations. In our example sites for instance, it clearly appears that when the texture gradient is short, as it was the case in Paracou, the texture-structure relationship (as measured by R^2) was not as strong as it was in areas covering a more extended gradient (as in Uppangala). Simulated images thus allowed us to place all plots and sites along a large gradient of canopy texture in order to stabilize the PCAs axes and thus to increase robustness of the texture-structure relationship, making it more universal than when fitted within sites. We therefore call for the collaborative construction of a pantropical database of 3D forest mockups, that could be incremented from plot data and local allometries in order to document all the particular situations encountered in tropical forests. These mockups could then be processed with DART in homogeneous acquisition conditions to produce arrays of canopy images of sufficient generality. The relevant simulated spectral bands could finally be assembled according to the specific characteristics of any of the VHSR sensors from which it could appear realistic to gather a very large array of real world, homogeneous images as to perform global scale canopy texture analysis. This would be a way to consolidate the reference gradients in canopy texture that emerged from our simulation results as

to benchmark real observations, i.e. canopy texture analyses performed from real canopy images. This perspective is a straightforward extension of the approach we introduced in the present paper, and that would lead us toward a robust operational texture-structure relationship from which accurate assessments of tropical forests AGB and carbon stocks could be produced.

Acknowledgments

Pierre Ploton was supported by an Erasmus Mundus PhD grant from the 2013–2016 Forest, Nature and Society (FONASO) doctoral program. Satellite images were acquired through the Forest project funded by the European Institute of Technology-Climate Knowledge & Innovation Community (grant N° PIN0040_2015-3.1-044_P032_01-01). Forest inventory data were collected with the support of the CoForTips project as part of the ERA-Net BiodivERsA 2011–2012 European joint call (ANR-12-EBID-0002), the IRD project PPR FTH-AC “Changements globaux, biodiversité et santé en zone forestière d’Afrique Centrale”, the IFPCAR project “Controlling for Uncertainty in Assessment of Forest Aboveground Biomass in the Western Ghats of India” (grant N° 4509-1), Eramet, the World Bank, WWF, the African Development Bank and the Center for Tropical Forest Science – Forest Global Earth Observatory (CTFS-ForestGEO) of the Smithsonian Tropical Research Institute. We are thankful to the Pallisco company for granting access to their concession, as well as local and national authorities in Cameroon, India and DRC. Numerical experiments benefited from high-performance computing resources of the Montpellier Bioinformatics Biodiversity platform and the SouthGreen bioinformatics platform.

Appendix A

Table A1

Distribution of forest inventory data among sampling sites. Tree dimensions collected in field plots include the diameter at breast height (D), tree height (H), trunk height (Ht) and crown diameter (Cd).

Source	Country	Site	Plot (ha)	Tree dimensions				Taxonomic identification (in %)			
				D	H	Ht	Cd	Species	Genus	Family	Unidentified
Bastin et al. (2014)	DRC	Malebo	28	10,092	10,092	0	0	96,5	3,5	0	0
Unpublished (IRD-AMAP/ENS)	Cameroon	Deng-Deng	15	7847	343	342	42	62,1	17	17	3,9
Rutishauser et al. (2016) & Vincent et al. (2012)	French Guyana	Paracou	85	53,685	2191	1667	1740	85,3	0	0	14,7
CTFS - Chuyong et al. (2004)	Cameroon	Korup	50	24,590	0	0	0	95,8	4	0,2	0
Unpublished (IRD-AMAP/ENS)	Cameroon	Djomedjo	10	4959	505	504	186	65,4	14,4	17,7	2,5
Unpublished (IRD-AMAP/ENS)	Cameroon	Lomié	8	3571	539	128	0	75,5	7,7	11,1	5,7
Unpublished (IRD-AMAP/ENS)	Cameroon	Mabounié	12	4475	592	525	113	53,4	19,2	24,4	3
Unpublished (IRD-AMAP/ENS)	Cameroon	Mindourou I	11	5163	908	559	306	61,6	16,8	15,1	6,5
Unpublished (IRD-AMAP/ENS)	Cameroon	Mindourou II	12	5598	920	667	233	56,4	26,2	11,7	5,7
Unpublished (IRD-AMAP/ENS)	Cameroon	Ngoila	6	2611	126	161	0	69,6	18,5	6,1	5,8
Unpublished (IRD-AMAP/ENS)	Cameroon	Nemeyong	5	2824	260	227	90	65,6	17,2	14,6	2,7
Ploton et al. (2012)	India	Uppangala	15	8220	1729	1722	1728	0	0	0	100 ^a
Pargal et al. (2017)	India	Yellapur	22	9156	5032	0	0	97,8	0,4	0	1,8

^a AGB values at Uppangala were computed using the average wood density of four 1-ha plots in the area (from Jeyakumar et al. in press).

References

- Allain, C., Cloitre, M., 1991. Characterizing the lacunarity of random and deterministic fractal sets. *Phys. Rev. A* 44, 3552.
- Antin, C., Péliissier, R., Vincent, G., Couteron, P., 2013. Crown allometries are less responsive than stem allometry to tree size and habitat variations in an Indian monsoon forest. *Trees* 27, 1485–1495. <http://dx.doi.org/10.1007/s00468-013-0896-7>.
- Asner, G.P., Martin, R.E., 2008. Spectral and chemical analysis of tropical forests: scaling from leaf to canopy levels. *Remote Sens. Environ.* 112, 3958–3970.
- Asner, G.P., Mascaro, J., Muller-Landau, H.C., Vieilledent, G., Vaudry, R., Rasamoelina, M., Hall, J.S., van Breugel, M., 2011. A universal airborne LiDAR approach for tropical forest carbon mapping. *Oecologia* 168, 1147–1160. <http://dx.doi.org/10.1007/s00442-011-2165-z>.
- Baccini, A., Goetz, S.J., Walker, W.S., Laporte, N.T., Sun, M., Sulla-Menashe, D., Hackler, J., Beck, P.S.A., Dubayah, R., Friedl, M.A., 2012. Estimated carbon dioxide emissions from tropical deforestation improved by carbon-density maps. *Nat. Clim. Chang.* 2, 182–185.
- Barbier, N., Couteron, P., 2015. Attenuating the bidirectional texture variation of satellite images of tropical forest canopies. *Remote Sens. Environ.* 171, 245–260. <http://dx.doi.org/10.1016/j.rse.2015.07.011>.

- doi.org/10.1016/j.rse.2015.10.007.
- Barbier, N., Couteron, P., Proisy, C., Malhi, Y., Gastellu-Etchegorry, J.-P., 2010. The variation of apparent crown size and canopy heterogeneity across lowland Amazonian forests. *Glob. Ecol. Biogeogr.* 19, 72–84.
- Barbier, N., Proisy, C., Véga, C., Sabatier, D., Couteron, P., 2011. Bidirectional texture function of high resolution optical images of tropical forest: an approach using LiDAR hillshade simulations. *Remote Sens. Environ.* 115, 167–179.
- Barbier, N., Couteron, P., Gastellu-Etchegorry, J.-P., Proisy, C., 2012. Linking canopy images to forest structural parameters: potential of a modeling framework. *Ann. For. Sci.* 69, 305–311. <http://dx.doi.org/10.1007/s13595-011-0116-9>.
- Baskerville, G.L., 1972. Use of logarithmic regression in the estimation of plant biomass. *Can. J. For. Res.* 2, 49–53. <http://dx.doi.org/10.1139/x72-009>.
- Bastin, J.-F., Barbier, N., Couteron, P., Adams, B., Shapiro, A., Bogaert, J., De Cannière, C., 2014. Aboveground biomass mapping of African forest mosaics using canopy texture analysis: toward a regional approach. *Ecol. Appl.* 24, 1984–2001.
- Bastin, J.-F., Barbier, N., Réjou-Méchain, M., Fayolle, A., Gourlet-Fleury, S., Maniatis, D., de Haulleville, T., Baya, F., Beeckman, H., Beina, D., 2015. Seeing Central African forests through their largest trees. *Sci Rep* 5. <http://dx.doi.org/10.1038/srep13156>.
- Boudon, F., Le Moguédec, G.L., 2007. Déformation asymétrique de houppiers pour la génération de représentations paysagères réalistes. *Rev. Electron. Francoph. Inform. Graph.* 1.
- Breiman, L., 2001. Random forests. *Mach. Learn.* 45, 5–32.
- Broadbent, E.N., Asner, G.P., Peña-Claros, M., Palace, M., Soriano, M., 2008. Spatial partitioning of biomass and diversity in a lowland Bolivian forest: linking field and remote sensing measurements. *For. Ecol. Manag.* 255, 2602–2616. <http://dx.doi.org/10.1016/j.foreco.2008.01.044>.
- Chave, J., Muller-Landau, H.C., Baker, T.R., Easdale, T.A., Steege, H. ter, Webb, C.O., 2006. Regional and phylogenetic variation of wood density across 2456 neotropical tree species. *Ecol. Appl.* 16, 2356–2367. [http://dx.doi.org/10.1890/1051-0761\(2006\)016\[2356:RAPVOW\]2.0.CO;2](http://dx.doi.org/10.1890/1051-0761(2006)016[2356:RAPVOW]2.0.CO;2).
- Chave, J., Coomes, D., Jansen, S., Lewis, S.L., Swenson, N.G., Zanne, A.E., 2009. Towards a worldwide wood economics spectrum. *Ecol. Lett.* 12, 351–366. <http://dx.doi.org/10.1111/j.1461-0248.2009.01285.x>.
- Chave, J., Réjou-Méchain, M., Búrquez, A., Chidumayo, E., Colgan, M.S., Delitti, W.B.C., Duque, A., Eid, T., Fearnside, P.M., Goodman, R.C., Henry, M., Martínez-Yrizar, A., Mugasha, W.A., Muller-Landau, H.C., Mencuccini, M., Nelson, B.W., Ngomanda, A., Nogueira, E.M., Ortiz-Malavassi, E., Péliissier, R., Ploton, P., Ryan, C.M., Saldarriaga, J.G., Vieilledent, G., 2014. Improved allometric models to estimate the aboveground biomass of tropical trees. *Glob. Chang. Biol.* 20, 3177–3190. <http://dx.doi.org/10.1111/gcb.12629>.
- Chuyong, G.B., Condit, R., Kenfack, D., Losos, E.C., Moses, S.N., Songwe, N.C., Thomas, D.W., 2004. Korup forest dynamics plot, Cameroon. *Trop. For. Divers. Dynamism* 506–516.
- Couteron, P., 2002. Quantifying change in patterned semi-arid vegetation by Fourier analysis of digitized aerial photographs. *Int. J. Remote Sens.* 23, 3407–3425.
- Couteron, P., Péliissier, R., Nicolini, E.A., Paget, D., 2005. Predicting tropical forest stand structure parameters from Fourier transform of very high-resolution remotely sensed canopy images. *J. Appl. Ecol.* 42, 1121–1128.
- Cressie, N.A., 1993. *Statistics for Spatial Data: Wiley Series in Probability and Mathematical Statistics*. (Find This Artic. Online).
- DeFries, R., Achard, F., Brown, S., Herold, M., Murdiyasar, D., Schlamadinger, B., de Souza, C., 2007. Earth observations for estimating greenhouse gas emissions from deforestation in developing countries. *Environ. Sci. Pol.* 10, 385–394.
- Dolédéc, S., Chessel, D., 1994. Co-inertia analysis: an alternative method for studying species–environment relationships. *Freshw. Biol.* 31, 277–294.
- Dray, S., Chessel, D., Thioulouse, J., 2003. Co-inertia analysis and the linking of ecological data tables. *Ecology* 84 (11), 3078–3089.
- Erdody, T.L., Moskal, L.M., 2010. Fusion of LiDAR and imagery for estimating forest canopy fuels. *Remote Sens. Environ.* 114, 725–737.
- Fayad, I., Baghdadi, N., Guitet, S., Baillly, J.-S., Hérault, B., Gond, V., El Hajj, M., Minh, D.H.T., 2016. Aboveground biomass mapping in French Guiana by combining remote sensing, forest inventories and environmental data. *Int. J. Appl. Earth Obs. Geoinf.* 52, 502–514.
- Feldpausch, T.R., Lloyd, J., Lewis, S.L., Brien, R.J., Gloor, M., Monteagudo Mendoza, A., Lopez-Gonzalez, G., Banin, L., Abu Salim, K., Affum-Baffoe, K., 2012. Tree height integrated into pantropical forest biomass estimates. *Biogeosciences* 3381–3403.
- Franklin, J.F., Spies, T.A., Van Pelt, R., Carey, A.B., Thornburgh, D.A., Berg, D.R., Lindenmayer, D.B., Harmon, M.E., Keeton, W.S., Shaw, D.C., 2002. Disturbances and structural development of natural forest ecosystems with silvicultural implications, using Douglas-fir forests as an example. *For. Ecol. Manag.* 155, 399–423.
- Frazer, G.W., Wulder, M.A., Niemann, K.O., 2005. Simulation and quantification of the fine-scale spatial pattern and heterogeneity of forest canopy structure: a lacunarity-based method designed for analysis of continuous canopy heights. *For. Ecol. Manag.* 214, 65–90.
- Gastellu-Etchegorry, J.-P., Yin, T., Laurent, N., Cajgfinger, T., Gregoire, T., Grau, E., Feret, J.-B., Lopes, M., Guilleux, J., Dedieu, G., 2015. Discrete Anisotropic Radiative Transfer (DART 5) for modeling airborne and satellite spectroradiometer and LiDAR acquisitions of natural and urban landscapes. *Remote Sens.* 7, 1667–1701.
- Guariguata, M.R., Ostertag, R., 2001. Neotropical secondary forest succession: changes in structural and functional characteristics. *For. Ecol. Manag.* 148, 185–206.
- Hajjem, A., Bellavance, F., Larocque, D., 2014. Mixed-effects random forest for clustered data. *J. Stat. Comput. Simul.* 84, 1313–1328.
- Haralick, R.M., 1979. Statistical and structural approaches to texture. *Proc. IEEE* 67, 786–804.
- ICRAF, 2007. Wood Density Database. World Agrofor. Cent., Nairobi Kenya. <http://db.worldagroforestry.org/wd>.
- Jeyakumar, S., Ayyappan, N., Muthuramkumar, S., Rajarathinam, K., Impacts of selective logging on diversity, species composition and biomass of residual lowland dipterocarp forest in central Western Ghats, India. *Trop. Ecol.* (in press).
- Jucker, T., Caspersen, J., Chave, J., Antin, C., Barbier, N., Bongers, F., Dalponte, M., van Ewijk, K.Y., Forrester, D.I., Haeni, M., Higgins, S.I., Holdaway, R.J., Iida, Y., Lorimer, C., Marshall, P.L., Momo, S., Moncrieff, G.R., Ploton, P., Poorter, L., Rahman, K.A., Schlund, M., Sonké, B., Sterck, F.J., Trugman, A.T., Usoltsev, V.A., Vanderwel, M.C., Waldner, P., Wedeux, B.M.M., Wirth, C., Wöll, H., Woods, M., Xiang, W., Zimmermann, N.E., Coomes, D.A., 2017. Allometric equations for integrating remote sensing imagery into forest monitoring programmes. *Glob. Chang. Biol.* 23 (1), 177–190.
- Lu, D., 2006. The potential and challenge of remote sensing-based biomass estimation. *Int. J. Remote Sens.* 27, 1297–1328.
- Lu, D., Chen, Q., Wang, G., Moran, E., Batistella, M., Zhang, M., Vaglio Laurin, G., Saah, D., 2012. Aboveground Forest biomass estimation with Landsat and LiDAR data and uncertainty analysis of the estimates. *Int. J. For. Res.* 2012, 1–16. <http://dx.doi.org/10.1155/2012/436537>.
- Malhi, Y., Román-Cuesta, R.M., 2008. Analysis of lacunarity and scales of spatial homogeneity in IKONOS images of Amazonian tropical forest canopies. *Remote Sens. Environ.* 112, 274–287.
- Mandelbrot, B.B., 1983. *The Fractal Geometry Of Nature*. Macmillan.
- Marvin, D.C., Koh, L.P., Lynam, A.J., Wich, S., Davies, A.B., Krishnamurthy, R., Stokes, E., Starkey, R., Asner, G.P., 2016. Integrating technologies for scalable ecology and conservation. *Glob. Ecol. Conserv.* 7, 262–275. <http://dx.doi.org/10.1016/j.gecco.2016.07.002>.
- Mascaro, J., Asner, G.P., Knapp, D.E., Kennedy-Bowdoin, T., Martin, R.E., Anderson, C., Higgins, M., Chadwick, K.D., 2014. A tale of two “forests”: random forest machine learning aids tropical forest carbon mapping. *PLoS ONE* 9, e85993. <http://dx.doi.org/10.1371/journal.pone.0085993>.
- Meng, S., Pang, Y., Zhang, Z., Jia, W., Li, Z., 2016. Mapping aboveground biomass using texture indices from aerial photos in a temperate Forest of Northeastern China. *Remote Sens.* 8, 230. <http://dx.doi.org/10.3390/rs8030230>.
- Mermoz, S., Réjou-Méchain, M., Villard, L., Le Toan, T., Rossi, V., Gourlet-Fleury, S., 2015. Decrease of L-band SAR backscatter with biomass of dense forests. *Remote Sens. Environ.* 159, 307–317. <http://dx.doi.org/10.1016/j.rse.2014.12.019>.
- Messinger, M., Asner, G., Silman, M., 2016. Rapid assessments of Amazon forest structure and biomass using small unmanned aerial systems. *Remote Sens.* 8, 615. <http://dx.doi.org/10.3390/rs8080615>.
- Morton, D.C., Cook, B.D., 2016. Amazon forest structure generates diurnal and seasonal variability in light utilization. *Biogeosciences* 13, 2195.
- Pan, Y., Birdsey, R.A., Fang, J., Houghton, R., Kauppi, P.E., Kurz, W.A., Phillips, O.L., Shvidenko, A., Lewis, S.L., Canadell, J.G., 2011. A large and persistent carbon sink in the world's forests. *Science* 333, 988–993.
- Pargal, S., Fararoda, R., Rajashekar, G., Balachandran, N., Réjou-Méchain, M., Barbier, N., Jha, C.S., Péliissier, R., Dadhwal, V.K., Couteron, P., 2017. Inverting aboveground biomass–canopy texture relationships in a landscape of Forest mosaic in the Western Ghats of India using very high resolution Cartosat imagery. *Remote Sens.* 9, 228.
- Ploton, P., Péliissier, R., Proisy, C., Flavenot, T., Barbier, N., Rai, S.N., Couteron, P., 2012. Assessing aboveground tropical forest biomass using Google Earth canopy images. *Ecol. Appl.* 22, 993–1003. <http://dx.doi.org/10.1890/11-1606.1>.
- Ploton, P., Barbier, N., Takoudjoo Momo, S., Réjou-Méchain, M., Boyemba Bosela, F., Chuyong, G., Dauby, G., Droissart, V., Fayolle, A., Goodman, R.C., Henry, M., Kamdem, N.G., Mukirania, J.K., Kenfack, D., Libalah, M., Ngomanda, A., Rossi, V., Sonké, B., Texier, N., Thomas, D., Zebaze, D., Couteron, P., Berger, U., Péliissier, R., 2016. Closing a gap in tropical forest biomass estimation: taking crown mass variation into account in pantropical allometries. *Biogeosciences* 13, 1571–1585. <http://dx.doi.org/10.5194/bg-13-1571-2016>.
- Proisy, C., Couteron, P., Fromard, F., 2007. Predicting and mapping mangrove biomass from canopy grain analysis using Fourier-based textural ordination of IKONOS images. *Remote Sens. Environ.* 109, 379–392.
- Proisy, C., Féret, J.-B., Laurent, N., Gastellu-Etchegorry, J.-P., 2016. Mangrove forest dynamics using very high spatial resolution optical remote sensing. In: Baghdadi, N.N., Zribi, M. (Eds.), *Remote Sensing of Land Surfaces: Urban and Coastal Area*, pp. 274–300 Paris.
- R Core Team, 2016. R: a language and environment for statistical computing. In: R Foundation for Statistical Computing, (Vienna, Austria). URL <https://www.R-project.org/>.
- Réjou-Méchain, M., Tymen, B., Blanc, L., Fauset, S., Feldpausch, T.R., Monteagudo, A., Phillips, O.L., Richard, H., Chave, J., 2015. Using repeated small-footprint LiDAR acquisitions to infer spatial and temporal variations of a high-biomass neotropical forest. *Remote Sens. Environ.* 169, 93–101.
- Réjou-Méchain, M., Tanguy, A., Piponiot, C., Chave, J., Hérault, B., 2017. Biomass: an R package for estimating above-ground biomass and its uncertainty in tropical forests. *Methods Ecol. Evol.* <http://dx.doi.org/10.1111/2041-210X.12753>.
- Rutishauser, E., Hérault, B., Petronelli, P., Sist, P., 2016. Tree height reduction after selective logging in a tropical forest. *Biotropica* 48 (3), 285–289.
- Saatchi, S.S., Harris, N.L., Brown, S., Lefsky, M., Mitchard, E.T., Salas, W., Zutta, B.R., Buermann, W., Lewis, S.L., Hagen, S., 2011. Benchmark map of forest carbon stocks in tropical regions across three continents. *Proc. Natl. Acad. Sci.* 108, 9899–9904.
- Schneider, F.D., Leiterer, R., Morsdorf, F., Gastellu-Etchegorry, J.-P., Laurent, N., Pfeifer, N., Schaepman, M.E., 2014. Simulating imaging spectrometer data: 3D forest modeling based on LiDAR and in situ data. *Remote Sens. Environ.* 152, 235–250. <http://dx.doi.org/10.1016/j.rse.2014.06.015>.
- Singh, M., Malhi, Y., Bhagwat, S., 2014. Biomass estimation of mixed forest landscape using a Fourier transform texture-based approach on very-high-resolution optical satellite imagery. *Int. J. Remote Sens.* 35, 3331–3349. <http://dx.doi.org/10.1080/>

- 01431161.2014.903441.
- Singh, M., Evans, D., Friess, D.A., Tan, B.S., Nin, C.S., 2015. Mapping above-ground biomass in a tropical forest in Cambodia using canopy textures derived from Google Earth. *Remote Sens.* 7, 5057–5076. <http://dx.doi.org/10.3390/rs70505057>.
- Slik, J.W., Paoli, G., McGuire, K., Amaral, I., Barroso, J., Bastian, M., Blanc, L., Bongers, F., Boundja, P., Clark, C., 2013. Large trees drive forest aboveground biomass variation in moist lowland forests across the tropics. *Glob. Ecol. Biogeogr.* 22, 1261–1271.
- Spies, T.A., 1998. Forest structure: a key to the ecosystem. *Northwest Sci.* 72, 34–36.
- Stark, S.C., Enquist, B.J., Saleska, S.R., Leitold, V., Schietti, J., Longo, M., Alves, L.F., Camargo, P.B., Oliveira, R.C., 2015. Linking canopy leaf area and light environments with tree size distributions to explain Amazon forest demography. *Ecol. Lett.* 18 (7), 636–645. <http://dx.doi.org/10.1111/ele.12440>.
- Taubert, F., Jahn, M.W., Dobner, H.-J., Wiegand, T., Huth, A., 2015. The structure of tropical forests and sphere packings. *Proc. Natl. Acad. Sci.* 112, 15125–15129.
- Véga, C., Vepakomma, U., Morel, J., Bader, J.L., Rajashekar, G., Jha, C.S., ... Dadhwal, V.K., 2015. Aboveground-biomass estimation of a complex tropical forest in India using lidar. *Remote Sens.* 7 (8), 10607–10625.
- Vieilledent, G., Gardi, O., Grinand, C., Burren, C., Andriamananjato, M., Camara, C., Gardner, C.J., Glass, L., Rasolohery, A., Rakoto Ratsimba, H., Gond, V., Rakotoarijaona, J.-R., 2016. Bioclimatic envelope models predict a decrease in tropical forest carbon stocks with climate change in Madagascar. *J. Ecol.* 104, 703–715. <http://dx.doi.org/10.1111/1365-2745.12548>.
- Vincent, G., Sabatier, D., Blanc, L., Chave, J., Weissenbacher, E., Péliissier, R., Fonty, E., Molino, J.-F., Couteron, P., 2012. Accuracy of small footprint airborne LiDAR in its predictions of tropical moist forest stand structure. *Remote Sens. Environ.* 125, 23–33.
- Vincent, G., Sabatier, D., Rutishauser, E., 2014. Revisiting a universal airborne light detection and ranging approach for tropical forest carbon mapping: scaling-up from tree to stand to landscape. *Oecologia* 175, 439–443. <http://dx.doi.org/10.1007/s00442-014-2913-y>.
- Vincent, G., Antin, C., Laurans, M., Heurtebize, J., Durrieu, S., Lavalley, C., Dauzat, J., 2017. Mapping plant area index of tropical evergreen forest by airborne laser scanning. A cross-validation study using LAI2200 optical sensor. *Remote Sens. Environment* 198, 254–266.
- Withmore, T.C., 1975. *Tropical Rain Forest of the Far East*. Clarendon Press Oxf. Univ. Press Lond.
- Wu, H., Zhang, J.-T., 2006. *Nonparametric Regression Methods for Longitudinal Data Analysis: Mixed-effects Modeling Approaches*. John Wiley & Sons.
- Xu, L., Saatchi, S.S., Yang, Y., Yu, Y., White, L., 2016. Performance of non-parametric algorithms for spatial mapping of tropical forest structure. *Carbon Balance Manag.* 11. <http://dx.doi.org/10.1186/s13021-016-0062-9>.
- Zanne, A.E., Lopez-Gonzalez, G., Coomes, D.A., Ilic, J., Jansen, S., Lewis, S.L., Miller, R.B., Swenson, N.G., Wiemann, M.C., Chave, J., 2009. Data from: towards a worldwide wood economics spectrum. In: Dryad Digital Deposit.
- Zhao, P., Lu, D., Wang, G., Wu, C., Huang, Y., Yu, S., 2016. Examining spectral reflectance saturation in Landsat imagery and corresponding solutions to improve forest aboveground biomass estimation. *Remote Sens.* 8, 469. <http://dx.doi.org/10.3390/rs8060469>.
- Zhou, J., Proisy, C., Descombes, X., Le Maire, G., Nouvellon, Y., Stape, J.-L., Viennois, G., Zerubia, J., Couteron, P., 2013. Mapping local density of young eucalyptus plantations by individual tree detection in high spatial resolution satellite images. *For. Ecol. Manag.* 301, 129–141.